MPMI Vol. 38, No. 6, 2025, pp. 1031–1043, https://doi.org/10.1094/MPMI-09-25-0125-R

RESEARCH

Multilevel Analysis of Response to Plant Growth-Promoting and Pathogenic Bacteria in Arabidopsis Roots

Anna Koprivova,[1] Miroslav Berka,[2] Veronika Berková,[2] Daniela Ristova,[1] Gözde Merve Türksoy,[1,3] Melina Schwier,[1] Philipp Westhoff,[4] Martin Černý,[2] and Stanislav Kopriva[1,†]

[1] Institute for Plant Sciences, Cluster of Excellence on Plant Sciences (CEPLAS), University of Cologne, Zülpicher Str. 47b, 50674 Cologne, Germany
[2] Department of Molecular Biology and Radiobiology, Faculty of AgriSciences, Mendel University in Brno, Zemědělská 1/1665, 613 00 Brno, Czech Republic
[3] Max Planck Institute for Plant Breeding Research, Carl-von-Linne-Weg 10, 50829 Cologne, Germany
[4] Plant Metabolism and Metabolomics Facility, Cluster of Excellence on Plant Sciences (CEPLAS), Heinrich Heine University Düsseldorf, 40225 Düsseldorf, Germany

Accepted for publication 20 September 2025.

A major challenge in plant–microbe interaction research is understanding how plants distinguish between commensal and pathogenic microorganisms. We compared Arabidopsis responses to two contrasting bacterial strains, the plant growth-promoting (PGP) *Pseudomonas* sp. CH267 and the pathogen *Burkholderia glumae* PG1, using integrated multi-omics analyses. The pathogen triggered stronger transcriptional reprogramming and proteomic changes in roots than the PGP strain, and both strains also affected numerous leaf proteins, indicating systemic responses. Interaction with both strains increased the abundance of sulfur-containing metabolites camalexin, glutathione, and cysteine, in particular under pathogen treatment, which corresponded with elevated total sulfur in the leaves. Root and root exudate metabolomes significantly changed, with amino acids and tricarboxylic acid cycle intermediates accumulating in roots but being diminished in the exudates. Integrative analysis across the omics datasets revealed strong correlations between metabolite levels, protein abundance, and transcript levels, highlighting new links between sulfur metabolism, defense pathways, and mineral nutrition, including iron. Together, these findings uncover the complex multilayered nature of Arabidopsis responses to commensal and pathogenic bacteria and identify new connections across different regulatory levels.

Keywords: *Arabidopsis thaliana*, integrative analysis, ionomics, metabolomics, plant–microbe interactions, proteomics, root exudates, transcriptomics

Plants in their natural habitats interact with a wide range of microorganisms, including both commensal and pathogenic species. To protect from pathogens, plants evolved a complex multilayered innate immunity system, including chemical defenses mediated by diverse phytoalexins. However, because both beneficial and pathogenic microbes are recognized by the same pattern-recognition receptors through conserved microbial structures, a central question remains: How does the plant immune system distinguish between commensals and pathogens (Ji et al. 2022; Thoms et al. 2021)? Indeed, even symbiotic microbes, such as mycorrhizal fungi and Rhizobia, initially trigger immune responses (Campos-Soriano et al. 2012) but subsequently are able to overcome them, such as through bacterial polysaccharides chelating calcium ions (Aslam et al. 2008) or the action of various effectors (de Jonge et al. 2010). Similarly, plant growth-promoting (PGP) bacteria also induce immunity-related genes (Teixeira et al. 2021) and at the same time modulate the expression of flagellin-elicited genes to suppress the plant immune response (Teixeira et al. 2021).

Many studies have revealed the beneficial effects of PGP strains on plant growth, nutrient supply, hormone production, and protection against pathogens (Haney et al. 2015; Kertesz and Mirleau 2004; Poupin et al. 2013). However, the molecular mechanisms of how these strains overcome the plant

[†]Corresponding author: S. Kopriva; skopriva@uni-koeln.de

Author contributions: S.K. and A.K. conceived and designed the research, A.K., M.B., V.B., G.M.T., M.S., and P.W. performed the experiments. A.K., M.B., D.R., M.S., M.Č., and S.K. analyzed the data. S.K. drafted the manuscript. A.K., M.B., M.Č., and S.K. prepared the figures. All authors were involved in revising the manuscript.

Data availability: The RNAseq data are available through the NCBI SRA repository under accession number PRJNA1196130. The mass spectrometry proteomics data were deposited at the ProteomeXchange Consortium with the dataset identifier PXD058537. Other data and materials are available from the corresponding author upon request.

Funding: This work was supported by the Deutsche Forschungsgemeinschaft (DFG) under Germany's Excellence Strategy – EXC 2048/1 – project 390686111 (S. Kopriva, A. Koprivova, D. Ristova, and P. Westhoff) and under Priority Programme "2125 Deconstruction and Reconstruction of Plant Microbiota (DECRyPT)," project 401836049 (S. Kopriva and G. M. Türksoy). M. Berka, V. Berková, and M. Černý acknowledge the support of the Czech-German mobility project 8J23DE004.

e-Xtra: Supplementary material is available online.

The author(s) declare no conflict of interest.

immune system remain largely elusive. Increasing evidence points to a central role of metabolic signaling in establishing symbiosis, either through selective effects of plant metabolites on specific microbes or reciprocal microbial signaling (Harbort et al. 2020; Huang et al. 2019; Sasse et al. 2018; Thoms et al. 2021; Zipfel and Oldroyd 2017). Indeed, for example, mutualistic interactions of Arabidopsis with endophytic fungi depend on fungal growth restriction by indolic glucosinolates and other indole-derived phytoalexins (Lahrmann et al. 2015). Accordingly, many plant metabolites with antimicrobial properties shape microbiome composition (reviewed in Jacoby et al. 2021). Among them, camalexin, a sulfur-containing indolic phytoalexin of the Brassicaceae, has long been studied as a defense metabolite induced by fungal and bacterial infection, but also by abiotic factors (Browne et al. 1991; Glawischnig 2007; Kliebenstein et al. 2005; Nguyen et al. 2022). However, camalexin is also important for microbiome function and PGP activity of various bacterial strains (Koprivova et al. 2019). Similarly, coumarins, which are toxic to many bacteria, influence microbiome composition, in particular under conditions of varying iron availability (Harbort et al. 2020; Stringlis et al. 2018).

Global omics approaches have begun to shed light on the mechanisms of plant colonization by commensal microbes. For instance, Arabidopsis leaves exposed to 39 bacterial strains displayed highly variable transcriptome and metabolome responses, yet a core set of 24 genes was induced by more than 70% of the strains, even across a large phylogenetic distance (Maier et al. 2021). These genes included *CYP71A12*, encoding the key enzyme in camalexin synthesis, as well as glutathione (GSH) S-transferases *GST6* and *GST7* and a peroxidase, *PRX71*, all genes associated with pathogen responses (Maier et al. 2021). Similarly, analysis of Arabidopsis roots inoculated with 36 bacterial and fungal strains revealed a conserved immunity-related transcriptional response, with upregulation of hypoxia-responsive genes and downregulation of genes for redox regulation (Hucklenbroich et al. 2021). At the metabolic level, tryptophan-derived secondary compounds consistently emerged as central players, in line with the known importance of camalexin and indolic glucosinolates for plant–microbe interactions (Maier et al. 2021). Despite these insights, integrative multi-omics analyses capturing plant responses to microbes across multiple levels are still scarce.

Here, we aimed to compare the Arabidopsis response to root inoculation with a PGP and a pathogenic bacterium. To this end, we selected *Pseudomonas* sp. CH267 and *Burkholderia glumae* PG1 as models. *Pseudomonas* sp. CH267 was isolated from roots of Arabidopsis grown in natural soil in Cambridge, Massachusetts, and promotes plant growth in a camalexin-dependent manner (Haney et al. 2015; Koprivova et al. 2019). *B. glumae* PG1 is a rice pathogen, causing panicle-blight disease (Ham et al. 2011). However, it also infects Arabidopsis, causing a large production of camalexin and a strong inhibition of root growth (Koprivova et al. 2023; Supplementary Fig. S1). Both strains can be used to treat plants in hydroculture (Koprivova et al. 2023), making them suitable models for comparative study.

We show that incubation with *Pseudomonas* sp. CH267 and *B. glumae* PG1 leads to extensive transcriptional reprogramming of the roots, different metabolite accumulation in roots and root exudates, changes in root and shoot proteomes, and alterations in shoot mineral composition, pointing to an importance of shoot root communication in plant–microbe interactions. Furthermore, integrative multi-omics analysis using Data Integration Analysis for Biomarker discovery using a Latent cOmponents (DIABLO) uncovered a multifaceted response revealing both shared and strain-specific features.

Results

Transcriptional response of Arabidopsis roots to different bacterial strains

As a first step to compare Arabidopsis responses to beneficial and pathogenic bacteria, we analyzed the root transcriptomes after inoculation with *Pseudomonas* sp. CH267 (hereafter CH267) and *B. glumae* PG1 (BG). We selected 3 days postinoculation as the sampling point, as previous experiments showed maximum camalexin exudation induced by CH267 at this time, and it was also the earliest time point at which camalexin accumulation differed in roots, shoots, and exudates between the two strains (Koprivova et al. 2023). Treatment with CH267 differentially regulated ($q < 0.01$, $|\log_2 FC| > 1$) 862 genes (636 upregulated and 226 downregulated), whereas BG caused a more significant transcriptional reprogramming, with 1,688 genes upregulated and 1,427 downregulated (Fig. 1A; Supplementary Table S1). Of the upregulated differentially expressed genes (DEGs), 392 were shared between the strains, representing 62% of CH267-induced DEGs but only 23% of BG-induced DEGs (Fig. 1A). CH267 upregulated most strongly peroxidases *PER4* and *PER28*, whereas BG mostly induced *Extensin 19* and *Alternative oxidase 1D* (Supplementary Table S1). Among the downregulated genes, 181 were common to both treatments, corresponding to 80% of CH267-repressed genes (Fig. 1A). Interestingly, 44 genes showed the opposite regulation: 37 were downregulated by BG and upregulated by CH267, including 4 peroxidases, the sugar transporter *STP4*, and nitrate transporter *NRT1*;*5*, whereas 7 genes showed the reverse pattern, for example, *Ferredoxin 1*, chalcone synthase *TT4*, and flavonol synthase *FLS1* (Fig. 1A; Supplementary Table S1).

Mapping the DEGs onto the MapMan metabolic map (Thimm et al. 2004) revealed that both strains affected similar pathways, with each containing both up- and downregulated genes (Supplementary Figs. S2 and S3). BG consistently affected a larger number of genes, particularly in categories related to pathogen defense and redox processes (Supplementary Fig. S4). In contrast, the CH267 responses were more strongly biased toward upregulation.

Gene Ontology (GO) and Kyoto Encyclopedia of Genes and Genomes (KEGG) enrichment analysis using Virtual Plant (Katari et al. 2010) revealed substantial functional overlap between the responses to the two strains. Shared upregulated categories included "response to other organism," "suberin biosynthetic process," "indole-containing compound metabolic process," and "glutathione transferase activity," whereas shared downregulated genes belonged to "photosynthesis," "response to stress," and "central vacuole" (Fig. 1B; Supplementary Table S2).

However, strain-specific responses were also evident. CH267 specifically induced genes related to "response to ethylene stimulus," "chitin binding," and "respiratory burst" while repressing many photosynthesis-related processes. BG specifically upregulated genes in "response to hormone stimulus," "ATPase activity," and "flavonoid metabolic process" and repressed categories linked to "cell growth," "circadian rhythm," and "carboxypeptidase activity" (Fig. 1B; Supplementary Table S2).

Consistently, KEGG pathways analysis showed shared enrichment in "amino acid metabolism," "phenylalanine metabolism," and "phenylpropanoid biosynthesis" (Supplementary Table S3). Additionally, BG specifically enriched "proteasome," whereas CH267 uniquely induced "valine, leucine and isoleucine degradation" and "plant-pathogen interaction." Both strains downregulated pathways related to "energy metabolism" and "photosynthesis." Interestingly, "phenylalanine metabolism" and "phenylpropanoid biosynthesis" appeared among both up- and downregulated DEGs, pointing to a

complex reprogramming of these pathways rather than a coordinated regulation (Supplementary Fig. S5; Supplementary Table S3).

Of particular interest were the categories enriched in genes with opposite regulation by CH267 and BG (Supplementary Table S1). Flavonoid biosynthesis, represented by *TT4* and *FLS1*, was enriched among BG-upregulated genes but repressed by CH267 (Table 1). Conversely, "peroxidase activity" and "heme binding" were overrepresented among CH267-upregulated but BG-repressed DEGs (Table 1). Correspondingly, KEGG pathway analysis confirmed the divergence with "flavonoid biosynthesis" enriched in BG-upregulated and CH267-downregulated DEGs, whereas "phenylalanine metabolism" and "phenylpropanoid biosynthesis" showed the opposite trend (Supplementary Figs. S2, S3, and S5; Supplementary Table S3). In summary, both CH267 and BG triggered extensive transcriptional reprogramming in Arabidopsis roots, with substantial overlap in core metabolic and defense pathways, showing a particular importance of amino acid, GSH, and flavonoid metabolism. BG induced broader and more balanced transcriptional changes, compared with the predominantly upregulating effect of CH267. Importantly, several functional categories and pathways, such as flavonoid biosynthesis, showed opposite regulation, reflecting the contrasting effects of beneficial and pathogenic bacteria on host gene expression.

Effect of treatment with pathogenic and PGP bacterial strains on Arabidopsis proteome

Next, we asked how far the changes we detected in transcripts are detectable at the proteome level. We analyzed Arabidopsis shoot and root proteomes of in all three conditions, mock and treatments with CH267 and BG, and identified and quantified

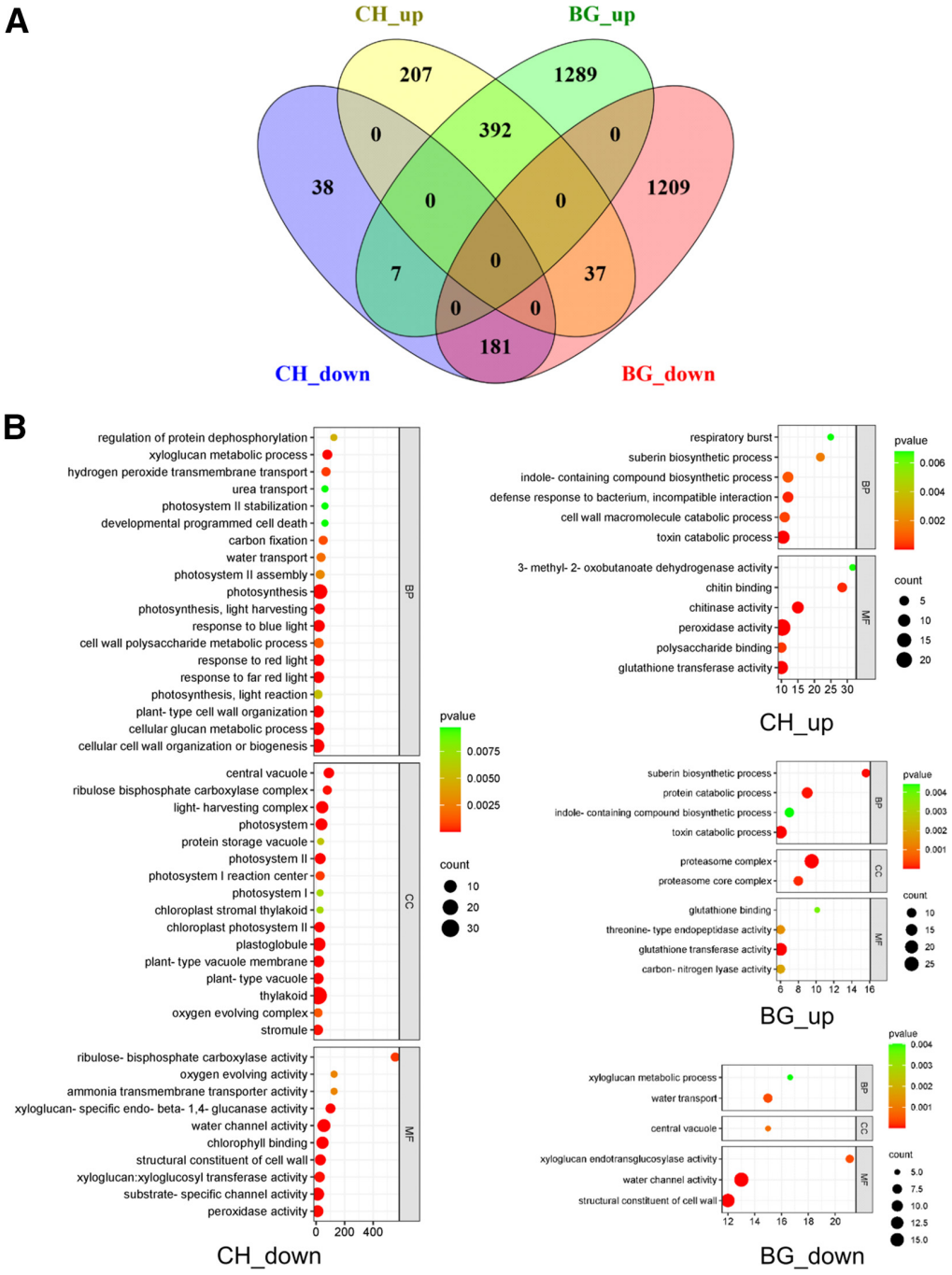

Fig. 1. Transcriptome response of Arabidopsis roots to *Pseudomonas* sp. CH267 (CH) and *Burkholderia glumae* PG1 (BG). **A,** Venn diagram showing the number of differentially expressed genes (DEGs) compared with mock treatment. **B,** Gene Ontology (GO) enrichment analysis. Shown are only GO terms enriched at least 10-fold, except the analysis of DEGs upregulated by BG, with a threshold of minimum sixfold. BR, biological process; CC, cellular compartment; MF, molecular function.

over 4,400 and 3,000 proteins, respectively. We compared the effect of the two bacterial strains on the proteomes, using stringent conditions of $q < 0.01$ and $|\log_2 FC| > 1$. As suggested by the RNA sequencing (RNAseq) results (Fig. 1A), both in roots and shoots, more differentially abundant proteins (DAPs) were found after treatment with BG than with CH267 (Fig. 2A). Similar to the transcriptome analysis, although some proteins were affected by both bacteria, more DAPs were specific to one strain. In the roots, 16 proteins were upregulated by both strains, whereas 101 and 12 were specific to BG and CH267, respectively. Further, 13 downregulated DAPs were shared, with 83 and 20 specifically downregulated by BG and CH267, respectively (Fig. 2A). In shoots, 53 proteins were more abundant under both treatments, whereas 80 and 43 were specific to BG and CH267, respectively.

Table 1. Enrichment analyses of Gene Ontology (GO) terms in differentially expressed genes from Arabidopsis roots upregulated in *Burkholderia glumae* and downregulated after treatment with the plant growth-promoting strain *Pseudomonas* sp. CH267

GO term	Observed frequency	Expected frequency	Enrichment	adj. *P* value	Category	Genes
Response to oxidative stress	5/34, 14.7%	247/22,304, 1.1%	13.4	0.00490	BF	AT5G19890 AT5G13930 AT1G49570 AT5G64100 AT2G18980
Lipid transport	3/34, 8.8%	137/22,304, 0.6%	14.7	0.03862	BF	AT4G12550 AT3G53980 AT4G33550
Lipid localization	3/34, 8.8%	153/22,304, 0.6%	14.7	0.03862	BF	AT4G12550 AT3G53980 AT4G33550
Flavonoid biosynthetic process	2/34, 5.8%	46/22,304, 0.2%	29.0	0.04573	BF	AT5G13930 AT5G08640
Flavonoid metabolic process	2/34, 5.8%	51/22,304, 0.2%	29.0	0.04841	BF	AT5G13930 AT5G08640
Cell wall	5/27, 18.5%	458/19,822, 2.3%	8.0	0.00729	CC	AT5G07030 AT5G47550 AT5G38940 AT5G64100 AT5G64120
External encapsulating structure	5/27, 18.5%	462/19,822, 2.3%	8.0	0.00729	CC	AT5G07030 AT5G47550 AT5G38940 AT5G64100 AT5G64120
Oxidoreductase activity, acting on peroxide as acceptor	5/41, 12.1%	103/24,443, 0.4%	30.3	0.00004	MF	AT5G19890 AT1G49570 AT5G64100 AT5G64120 AT2G18980
Peroxidase activity	5/41, 12.1%	103/24,443, 0.4%	30.3	0.00004	MF	AT5G19890 AT1G49570 AT5G64100 AT5G64120 AT2G18980
Antioxidant activity	5/41, 12.1%	130/24,443, 0.5%	24.2	0.00008	MF	AT5G19890 AT1G49570 AT5G64100 AT5G64120 AT2G18980
Electron carrier activity	5/41, 12.1%	427/24,443, 1.7%	7.1	0.01756	MF	AT5G19890 AT1G49570 AT5G64100 AT2G18980 AT1G10960
Heme binding	4/41, 9.7%	290/24,443, 1.1%	8.8	0.02632	MF	AT5G19890 AT1G49570 AT5G64100 AT2G18980
Tetrapyrrole binding	4/41, 9.7%	314/24,443, 1.2%	8.1	0.02632	MF	AT5G19890 AT1G49570 AT5G64100 AT2G18980
Iron ion binding	4/41, 9.7%	352/24,443, 1.4%	6.9	0.03354	MF	AT5G19890 AT1G49570 AT5G64100 AT2G18980
Lipid binding	3/41, 7.3%	173/24,443, 0.7%	10.4	0.03354	MF	AT4G12550 AT3G53980 AT4G33550

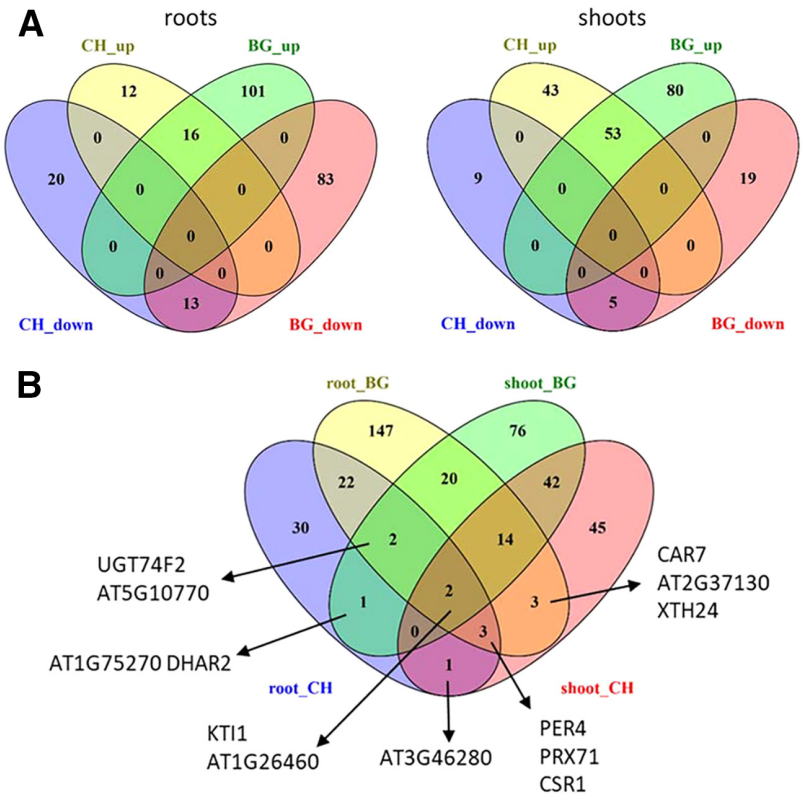

Fig. 2. Proteome response of Arabidopsis to *Pseudomonas* sp. CH267 (CH) and *Burkholderia glumae* PG1 (BG). **A,** Venn diagrams showing the number of differentially abundant proteins (DAPs) in roots and shoots after treatments with CH and BG. **B,** Venn diagram showing comparison of root and shoot DAPs after treatment with CH and BG.

In contrast, only 5 proteins were downregulated by both strains (Fig. 2A).

Comparing the proteomes in roots and shoots, only two proteins were induced by both strains in both organs, the Kunitz trypsin protease inhibitor KTI1 (AT1G73260) and the tetratricopeptide repeat (TPR)-like superfamily protein AT1G26460 (Fig. 2B). Thirty-eight DAPs were common in shoots and roots after treatment with BG, whereas only six proteins were common in both organs in plants treated with CH267, among them peroxidases PER4 and PRX71 and acetolactate synthase CSR1, involved in synthesis of branched amino acids (Fig. 2B).

Functional enrichment analysis revealed that in roots, both bacteria upregulated proteins linked to stress and defense, with BG additionally affecting metabolic pathways such as "carboxylic acid catabolic process" and "indole-3-acetonitrile nitrilase activity," whereas CH267 mainly enriched peroxidase and "antioxidant activity" (Supplementary Fig. S6; Supplementary Table S5), consistent with results of transcriptional analysis. BG downregulated translation-related proteins, whereas CH267 affected processes connected to cytoskeleton and chloroplasts, as observed in the RNAseq data (Supplementary Fig. S6; Supplementary Table S5). Correspondingly, among the BG-induced DAPs, KEGG pathways "amino acid metabolism," "valine, leucine and isoleucine degradation," "biosynthesis of other secondary metabolites," and "phenylalanine metabolism" were induced, the latter two also in the 16 proteins upregulated by both strains (Supplementary Table S6).

Also in shoots, both bacteria induced defense- and metabolism-related proteins (Supplementary Fig. S7; Supplementary Table S5), but BG specifically induced proteins involved in glucosinolate and serine biosynthesis, whereas proteins induced by CH267 were enriched in fatty acid metabolism, peroxidase activity, and heme binding (Supplementary Fig. S7; Supplementary Table S5). The KEGG pathway "amino acid metabolism" was induced in shoots on the protein level by both bacteria (Supplementary Table S6). We then compared the DEGs and DAPs in the roots. From the 117 proteins upregulated by BG, 59 (50.4%) corresponded to DEGs upregulated in the RNAseq analysis (Supplementary Fig. S8; Supplementary Table S7), whereas among the downregulated DAPs, it was 17.7%, with an additional 8 DAPs corresponding to upregulated DEGs (Supplementary Fig. S8). For CH267, 42.8% DAPs were upregulated on both the protein and mRNA levels, whereas only 15.2% were downregulated (Supplementary Table S7). The high level of overlap between DAPs and DEGs is reflected also in the enrichment analyses, because, for example, GO terms such as "glutathione binding," "glutathione transferase activity," and "indole-containing compound biosynthetic process" were found enriched among both upregulated DEGs and DAPs after treatment with BG (Fig. 1; Supplementary Fig. S6).

These results demonstrate that transcriptome changes are, to a large extent, mirrored at the protein level, particularly in defense- and metabolism-related pathways. The proteins induced by both bacterial strains—such as peroxidases and enzymes of secondary metabolism—likely represent a core response to microbial presence, independent of microbial lifestyle. In contrast, the much broader proteomic reprogramming triggered by BG, including suppression of translation-related proteins and induction of amino acid catabolism, reflects a pathogen-specific strategy that imposes greater metabolic costs on the host. By comparison, CH267 mainly enhanced antioxidant and peroxidase activity, suggesting a more selective adjustment that supports compatibility rather than defense activation. The limited overlap between DEGs and DAPs further highlights post-transcriptional regulation and organ-specific tuning. Together, these findings suggest that Arabidopsis mounts a shared basal proteomic response to both commensal and pathogenic bacteria, and additional layers of regulation distinguish beneficial from harmful interactions.

Treatment with CH267 and BG affects metabolite composition of the roots and exudates and shoot ionome

We next quantified metabolites from Arabidopsis roots and shoots after treatment with CH267, BG, or mock. Camalexin and related sulfur-containing metabolites were strongly affected: both CH267 and BG increased camalexin accumulation in roots and shoots, with BG inducing much higher levels (Fig. 3A). Cysteine and GSH, the latter representing the donor of sulfur for camalexin synthesis, were also elevated. Cysteine concentration doubled in roots treated with CH267 and tripled after incubation with BG but was increased only in pathogen-treated shoots (Fig. 3B). GSH followed a similar pattern and was induced by CH267 only in roots (Fig. 3C). In contrast, glucosinolates, involved in immunity similar to camalexin, were not affected in roots, but indolic glucosinolates were less abundant in shoots (Supplementary Fig. S9). Thus, CH267 and especially BG treatments triggered alterations in sulfur metabolism, agreeing with transcript and protein results.

To explore broader metabolic changes, we quantified 50 primary metabolites in roots. Most were significantly altered, with BG having a stronger effect (Fig. 4A). Indeed, BG increased α-ketoglutarate content 154-fold and alanine over 20-fold (Fig. 4A; Supplementary Table S8). Several metabolites, including tryptophan, methionine, phenylalanine, serine, threonine, and TCA cycle intermediates (fumarate, isocitrate, and malate), were elevated by both strains to similar levels, consistent with transcriptomic and proteomic results (Fig. 4A). Besides α-ketoglutarate and alanine, BG increased amino acids (ß-alanine, valine, asparagine, and tyrosine), organic acids (glycerate and threonate), and sugars (glucose and xylose) more strongly than CH267. Interestingly, accumulation of several sugars was differently affected by the two strains: raffinose, sucrose, and fructose decreased in CH267-treated roots but increased with BG (Fig. 4A; Supplementary Table S8).

Because root exudates are key for plant communication with microbes (Sasse et al. 2018), we also analyzed compounds secreted to a growth medium. Sixty-one metabolites were detected, about a half of them overlapping with the root metabolites. Most metabolites were exuded already from mock-treated plants, except trans-ferulic acid, 5-aminolevulinic acid, and allantoin (Supplementary Table S8). Interestingly, although roots generally accumulated metabolites upon bacterial treatments, their levels in exudates often decreased. Still, several compounds, such as indole 3-carboxylic acid, putrescine, thymine, and anthranilate, were more abundant in exudates after both treatments, whereas others (myo-inositol, asparagine, malate, and fumarate) declined (Fig. 4B). Interestingly, γ-aminobutyrate and uracil were less abundant in exudates of CH267-treated plants than in mock but increased with BG.

Because the bacterial treatments induced several genes related to nutrient uptake and homeostasis, such as *IRT1*, copper transport protein family (*AT5G52710*), phosphate transporter *PT3*;*2*, or *NRT1*;*8* (Supplementary Table S1), we examined nutrient contents in the shoots. Indeed, both strains altered elemental composition (Fig. 5; Supplementary Table S9). Boron and magnesium decreased with both, whereas potassium increased with CH267 but declined with BG. Iron, sulfur, and zinc accumulated to higher levels with CH267, whereas manganese increased and Mo decreased with BG (Fig. 5). Overall, treatments with both beneficial and pathogenic bacteria triggered extensive reprogramming of plant metabolism, exudation patterns, and nutrient homeostasis, with BG exerting stronger and broader effects than CH267.

Multilevel analysis of bacterial impact on Arabidopsis

To integrate the different global datasets, we applied the DIABLO framework (Singh et al. 2019). Partial least squares-discriminant analysis (PLS-DA) confirmed clear separation of mock, CH267, and BG treatments across all six datasets (i.e., root transcriptome, root and shoot proteomes, root metabolome, exudate metabolome, and shoot ionome) (Supplementary Fig. S10). The transcriptome dataset showed the strongest separation, whereas the root metabolome was the least distinct. From these analyses, we identified the genes and proteins contributing most to the treatment differences (Supplementary Fig. S11). The top 20 genes included genes for caffeoyl-CoA 3-O-methyltransferase, SUI1 family translation initiation factor, PHT1;9, or SNRK2.9. Key proteins included root enzymes, such as 3-phosphoserine phosphatase, aspartate aminotransferases 1 and 3, flavanone 3-hydroxylase, and glutamate dehydrogenase 2, as well as shoot proteins, including several GSH S-transferases, 3 peroxidases, and tryptophan synthase beta-subunit 1.

To explore cross-omics relationships, we calculated Spearman's correlation coefficients (Supplementary Table S10) and visualized them as clustered correlation matrices using ClustVis (Fig. 6A). Six major clusters emerged, each integrating features from multiple datasets. Cluster 1 grouped root proteins, such as tubulin beta 8 and polyribonucleotide nucleotidyltransferase, which were less abundant in CH267-treated roots, with reduced accumulation of sinapate and fructose in the roots and lower leaf calcium (Fig. 6A). Cluster 2 contained exuded metabolites, less abundant with both strains, such as glucose, myo-inositol, or malate, together with lower shoot magnesium and boron, as well as root proteins, including heat shock protein 91 and ribosomal protein S27. Cluster 3 was the largest and most heterogenous, combining exuded secondary compounds (e.g., salicylate, allantoin, anthranilate, and brassinin); defense-associated leaf proteins, such as leucine-rich repeat protein kinase AT2G26730, aspartyl protease family protein AT5G48430, xyloglucan endotransglucosylase XTH22, and protein kinase SIF1; leaf iron and sulfur; and root transcripts for CPK27 and SNRK2.4 (Fig. 6A). Cluster 4 grouped several shoot proteins (e.g., the 3 GSH S-transferases and tryptophan synthase beta-subunit 1) that were more abundant after both bacterial treatments with root metabolites, such as phenylalanine, tryptophan, isoleucine, and putrescine. Cluster 5 included transcripts induced by both strains but with a stronger effect from BG, as well as root proteins, including glutamate dehydrogenase 2 and aspartate aminotransferase 3. Finally, cluster 6 consisted exclusively of metabolites, such as glycerate, α-ketoglutarate, and maltose, along with sorbitol and rhamnose in exudates, all more abundant specifically upon BG treatment.

To highlight the strongest associations, we visualized correlations above 0.8 in a Circos plot (Fig. 6B). These links highlight the complexity of plant responses to microbial interactions.

Interestingly, the leaf proteome showed extensive correlations with root transcriptomic and metabolic changes, underscoring systemic coordination of the responses between shoots and roots.

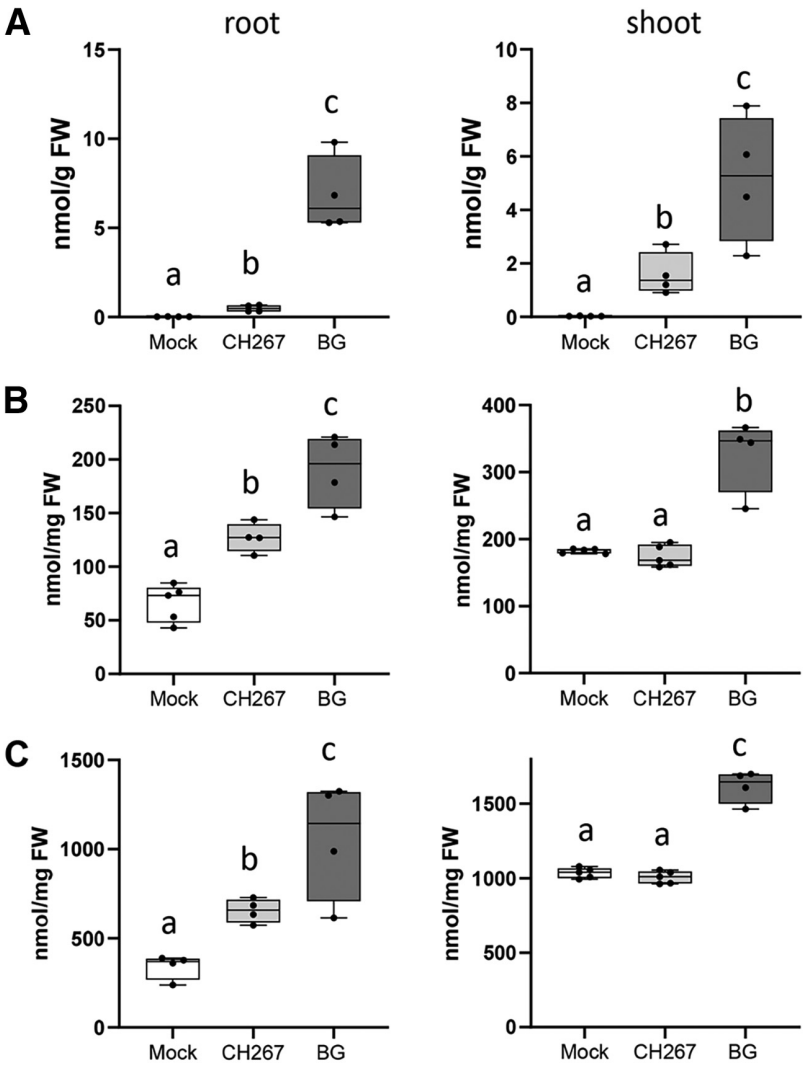

Fig. 3. Sulfur-containing metabolites in response of Arabidopsis to *Pseudomonas* sp. CH267 (CH267) and *Burkholderia glumae* PG1 (BG). Metabolites were analyzed in roots and shoots of Arabidopsis plants treated with CH267 or BG for 3 days by high-performance liquid chromatography. **A,** Camalexin. **B,** Cysteine. **C,** Glutathione. Different letters represent significant differences between the treatments at $P < 0.05$ (one-way analysis of variance; $n = 4$). FW, fresh weight.

In addition, several elements displayed multiple strong associations with protein and transcript abundances, pointing to a central role of nutrient homeostasis in shaping plant–microbe interactions.

Altogether, the integrative omics analysis uncovered strong correlations between transcripts, proteins, and metabolites and revealed new candidate nodes of regulation, such as linking sulfur and phenylpropanoid metabolism or iron with zinc transporters. The analysis thus revealed that the plant response to bacteria is not just modular but networked across multiple regulatory layers.

Discussion

Despite significant progress in deciphering plant responses to individual microbes and microbial communities, how plants distinguish between the commensal and pathogenic strains is not completely understood (Ji et al. 2022; Paries and Gutjahr 2023). In particular, although immunity is clearly crucial to plant responses to different microorganisms (Teixeira et al. 2021), new components are still being identified (Koprivova et al. 2019). Integrating global omics approaches offers a powerful strategy to uncover regulatory networks and novel components of plant–microbe interactions (Jain et al. 2024). To this end, we determined the Arabidopsis response to two contrasting bacterial strains across transcriptome, proteome, metabolome, and ionome levels.

Transcriptomics studies showed that diverse bacterial strains strongly affect plant gene expression in both leaves and roots (Maier et al. 2021; Nobori et al. 2022; Teixeira et al. 2021). Even among commensals, responses vary widely, with a little overlap. Maier et al. (2021) defined a core set of 24 genes consistently induced in Arabidopsis leaves by most of 39 studied

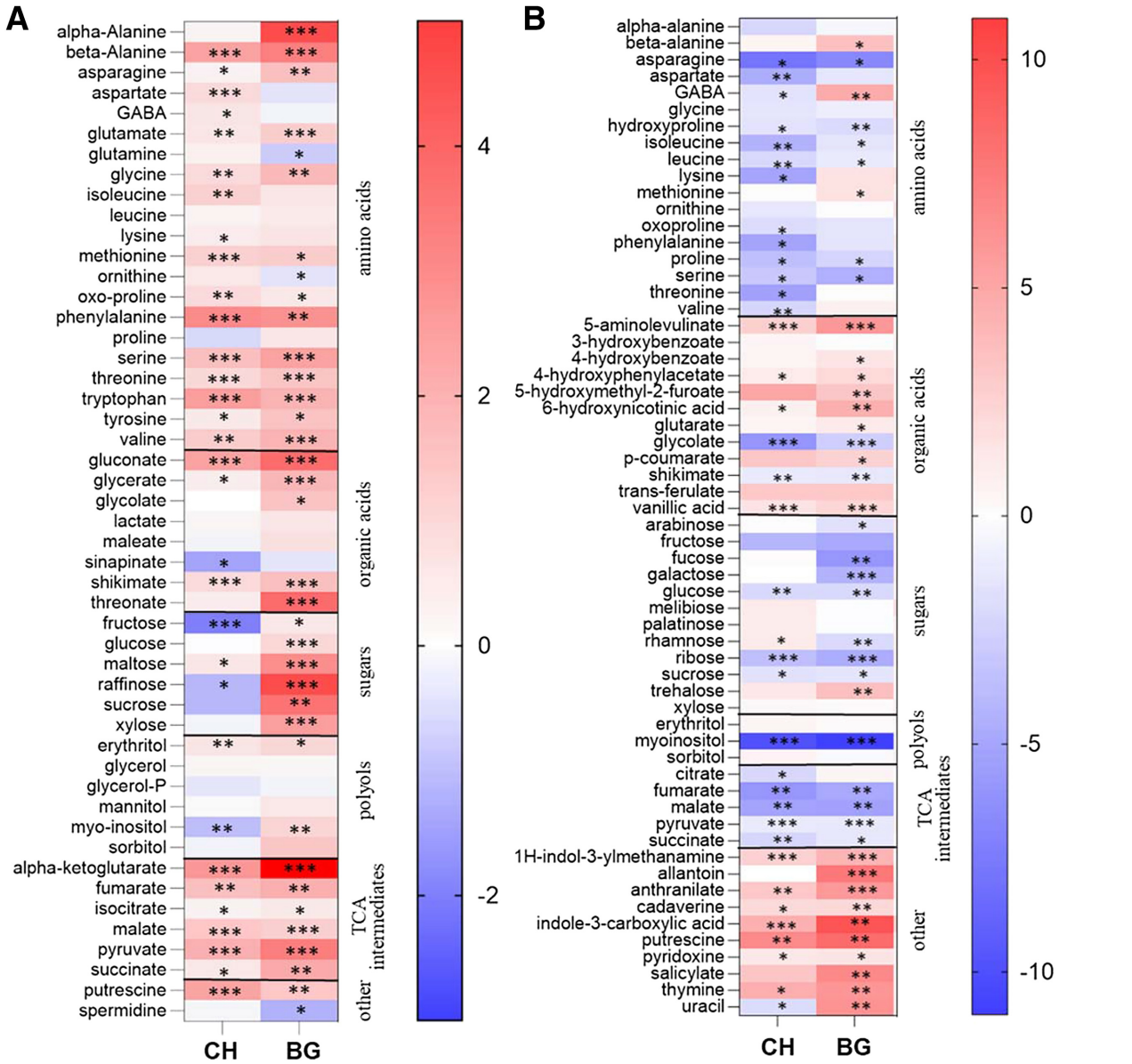

Fig. 4. Metabolite analysis of response of Arabidopsis to *Pseudomonas* sp. CH267 (CH) and *Burkholderia glumae* PG1 (BG). **A,** Metabolites were determined in Arabidopsis roots treated with mock, CH, or BG by gas chromatography-mass spectrometry (GC-MS). **B,** Exudates were collected from the treated plants and subjected to metabolite analysis by GC-MS. The heat maps show the $\log_2$ fold change between bacteria-treated plants and mock. Asterisks represent significant differences between bacterial treatments and mock (*t* test, $^*P < 0.05$, $^{**}P < 0.01$, $^{***}P < 0.001$). The data underlying the heatmap are presented in Supplementary Table S8.

commensal strains (Maier et al. 2021). Of these 24 genes, 13 were upregulated in the roots by CH267 and 8 by BG, with 7 in common, indicating conservation of responses to bacteria across tissues and an overlap between responses to pathogenic and commensal strains. However, as seen in other studies (Teixeira et al. 2021; Zhao et al. 2019), the pathogen BG affected many more genes than the PGP strain CH267 (Fig. 1). This was evident after mapping the DEGs across general metabolism, as well as focusing on stress response (Supplemental Figs. S2 to S4). Similar to other bacterial strains, both CH267 and BG induced genes from defense-related functional categories, such as synthesis of indolic compounds, similar to responses triggered by the flg22 peptide (Teixeira et al. 2021). Nevertheless, strain-specific signatures emerged: ethylene and jasmonate signaling were induced by CH267, whereas those connected to abiotic stress and abscisic acid were induced by BG (Supplementary Table S2). This is consistent with jasmonate and ethylene signaling being upregulated during *Pseudomonas simiae* WCS417r-induced systemic resistance against herbivores and tolerance to salt stress caused by *Enterobacter* sp. SA187 being dependent on ethylene (de Zélicourt et al. 2018; Pangesti et al. 2016). CH267 also induced genes for suberin biosynthesis, consistent with the importance of the endodermis barrier in shaping the microbiome (Salas-González et al. 2021). Both endodermal barrier formation and synthesis of tryptophan-derived metabolites were found to be key for host responses to root microbes in recent RNAseq analysis of cell type-specific root response to microbiota (Yang et al. 2025). The 44 genes oppositely regulated by the two strains and hypothesized to explain the different plant responses were enriched for phenylpropanoid synthesis. Notably, BG specifically upregulated flavonoid synthesis, whereas this pathway was repressed by CH267 (Table 1; Supplementary Fig. S5). Flavonoids are commonly found in root exudates and play important roles in plant interactions with other organisms (Ghitti et al. 2022). Remarkably, although there was only very small overlap in functional categories enriched in DEGs after treatment with BG of Arabidopsis roots and rice leaves, the two genes involved in flavonoid metabolism, *TT4* and *FLS1*, were induced in both (Table 1; Magbanua et al. 2014). Because flavonoids inhibit the production of the bacterial toxin toxoflavin in BG (Castellanos et al. 2020), upregulation of flavonoid synthesis might be a specific mechanism of plant defense against BG.

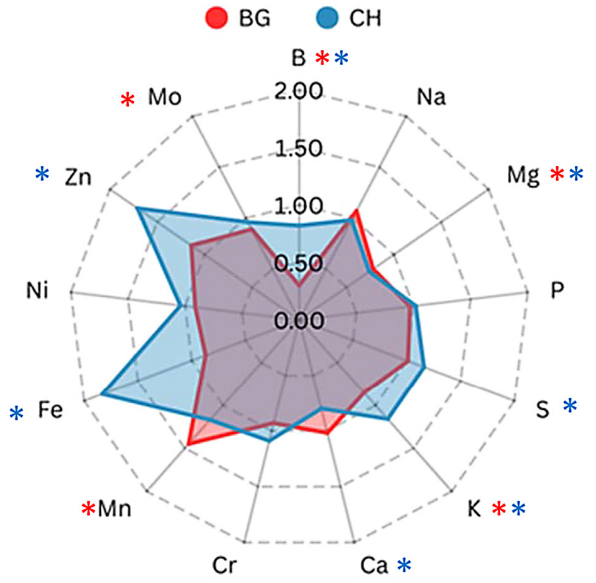

Fig. 5. Analysis of response of Arabidopsis leaf ionome to *Pseudomonas* sp. CH267 (CH) and *Burkholderia glumae* PG1 (BG). The concentrations of elements were determined in Arabidopsis shoots treated with mock, CH, or BG by inductively coupled plasma mass spectrometry. The spider graph shows the $\log_2$ fold change between bacteria-treated plants and mock. Asterisks represent significant differences between bacterial treatments (red BG, blue CH) and mock at $P < 0.05$ (*t* test). The data underlying the heatmap are presented in Supplementary Table S9.

Proteomic analysis revealed that both strains profoundly affected protein abundance, underscoring the importance of studying plant responses beyond the transcriptome (Fig. 2). As in the transcriptomic analysis, BG triggered more extensive proteomic changes than the PGP strain. Functional categories affected by CH267 and BG, particularly those related to defense and amino acid metabolism, mirrored patterns reported for other PGP strains (Kwon et al. 2016; Witzel et al. 2017). Interestingly, although the proteomic response to BG and CH267 significantly overlapped (Fig. 2A), BG did not regulate any proteins affected by a pathogenic protozoan, *Plasmodiophora brassicae*, despite both organisms activating defense (Devos et al. 2006). Remarkably, bacterial inoculation of the roots caused major proteomic shifts in leaves (Fig. 2), consistent with systemic signaling, such as during induced systemic resistance (Haney et al. 2018; Marzorati et al. 2023; Pieterse et al. 1996). Interestingly, CH267 and BG responses overlapped more than those of CH267 and another PGP strain, WCS417r, despite both being *Pseudomonas*. This suggests that environmental and growth conditions strongly influence outcomes of plant–microbe interactions, at least in terms of DAPs. Although the stringent statistical thresholds used in this study might have limited overlap detection, the observed patterns highlight the complexity of systemic proteomic responses.

The interaction of Arabidopsis with CH267 and BG also resulted in large alterations in the root metabolome and in the composition of root exudates. The metabolomic analyses emphasized the importance of sulfur and sulfur metabolites for plant interaction with bacteria (Mukherjee et al. 2025; Rausch and Wachter 2005; Wang et al. 2022). Both strains induced accumulation of sulfur-containing compounds (Fig. 3). Camalexin is one of the most prominent metabolites in Arabidopsis interaction with pathogens and PGP bacteria (Koprivova and Kopriva 2022), and correspondingly, camalexin was induced by both BG and CH267. BG triggered higher camalexin levels compared with CH267, matching the stronger transcriptional and proteomic induction of biosynthetic enzymes (Supplementary Tables S1 and S4). Similarly, GSH synthesis was induced on all three levels, reflecting its requirement for the increased camalexin synthesis and corresponding to induction of genes and proteins involved in GSH binding and GSH transferase activity (Supplementary Figs. S2, S6, and S7). Glucosinolates, which are also part of plant immunity, were only partly affected by the bacteria (Supplementary Fig. S9). This was somewhat surprising, because aliphatic glucosinolates were previously associated with defense specifically against bacterial pathogens (Fan et al. 2011). Indolic glucosinolates were reduced in shoots of BG-treated plants, possibly reflecting redirection of sulfur and indolic intermediates toward camalexin and consistent with increased accumulation of glucosinolate catabolic proteins (Supplementary Fig. S7). Altogether, these findings reinforce the central role of sulfur in plant defense (Rausch and Wachter 2005; Wang et al. 2022). Induction of genes involved in sulfur homeostasis (Supplementary Table S2) and increased accumulation of sulfur upon BG treatment (Fig. 5) further support this conclusion.

Amino acid metabolism was strongly affected, particularly under BG treatment. Amino acid catabolism was enriched on both the transcriptomic and proteomic levels, and catabolic products, such as cadaverine derived from lysine, were increased in the exudates, in agreement with the importance of amino acid metabolism in plant–microbe interactions (Moormann et al. 2022). However, roots accumulated amino acids, whereas

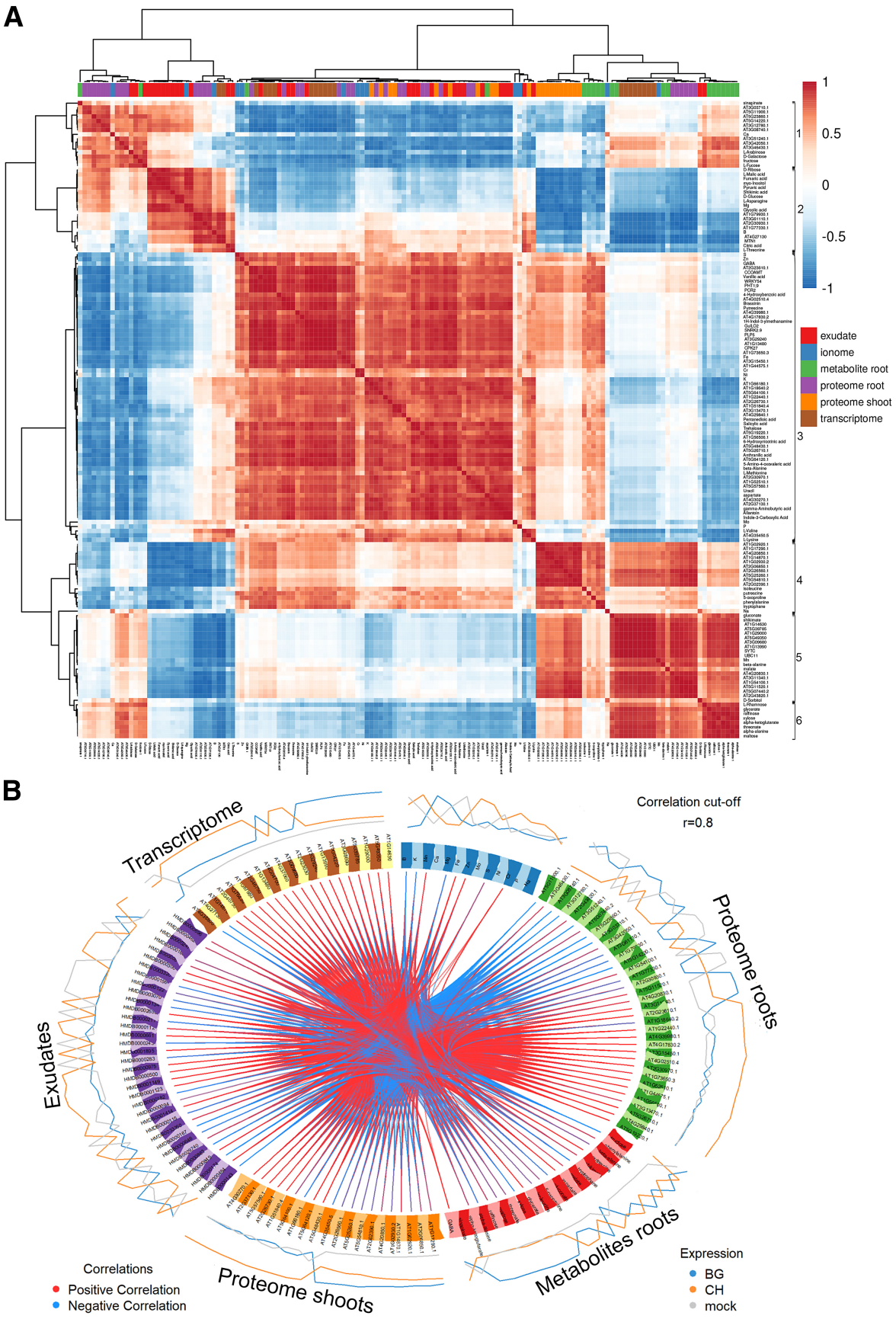

Fig. 6. Multilevel analysis of response of Arabidopsis to *Pseudomonas* sp. CH267 (CH) and *Burkholderia glumae* PG1 (BG). The DIABLO method was used to reduce the omics datasets into subsets of the most informative genes. Spearman's correlation coefficients were calculated to identify the relationships between the responses of the individual components to the two bacterial strains. **A,** The correlation matrix was subjected to hierarchical clustering. The heatmap represents the correlation coefficients, separated into six clusters. **B,** Circos plot of the correlations between components of the different datasets. Red links mark positive correlations, and blue links indicate negative correlations. The cut-off for the links was $|r| > 0.8$.

exudates contained fewer, suggesting that reduced exudation might contribute to the accumulation in root tissues (Fig. 4). The reduced exudation might suggest a reduction of carbon and nitrogen release to the rhizosphere, possibly as a defense strategy to limit pathogen growth. Downregulation of ribosomal proteins and proteins connected to translation in BG-treated roots (Supplementary Fig. S6) indicates a reduced protein synthesis rate and contribution to accumulation of amino acids. Exudation of myo-inositol, known to improve colonization by some PGP strains (Vilchez et al. 2020), was repressed by both CH267 and BG (Fig. 4), suggesting that myo-inositol is not a universal bacterial signal. On the contrary, indole 3-carboxylic acid exudation increased, corresponding to the upregulation of tryptophan metabolism on both the transcriptome and proteome levels (Fig. 4; Supplementary Fig. S6). However, although the metabolite changes were extensive, they were not able to fully explain the contrasting plant responses, pointing to the need for time-resolved studies.

Ionomic analyses revealed further distinctions (Fig. 5). CH267 increased iron and zinc in leaves, correlating with *IRT1* induction (Fig. 5; Supplementary Table S1). This is in accord with the recent finding of increased iron uptake in Arabidopsis roots colonized by *Pseudomonas putida* (Esparza-Reynoso et al. 2024). The iron connection is especially interesting because of the general role of iron in plant immunity (Herlihy et al. 2020) and because iron availability often governs microbial competition in the rhizosphere (Harbort et al. 2020). Other nutrient shifts, such as decreased boron and magnesium with both strains, or opposite effects on potassium (Fig. 5) and correlations between elemental concentrations and transcript and/or protein levels (Fig. 6) highlight micronutrient homeostasis as an integral component of plant–microbe interactions, an area requiring further exploration.

Comparing the individual analyses revealed widespread correlations of protein abundances with transcript levels (Supplementary Fig. S8) and accumulation of indolic metabolites and expression of genes of the tryptophan network. Further insights into Arabidopsis responses were provided through integrating transcriptomic, proteomic, metabolomic, and ionomic datasets with DIABLO, which enables the reduction of complex datasets to a subset of the most informative features (Singh et al. 2019). This approach is widely use to integrate diverse omics analyses, such as transcriptomics, proteomics, and metabolomics, or data from complex time course experimental designs (Bancel et al. 2019; Burton-Pimentel et al. 2021). The analysis highlighted sulfur metabolism, phenylpropanoid biosynthesis, and amino acid metabolism as central pathways, and subsequent hierarchical clustering revealed coordinated responses across roots and shoots. For example, zinc accumulation clustered with expression of the *PLANT CADMIUM RESISTANCE 2* (*PCR2*) gene for a zinc exporter (Song et al. 2010). The frequent correlation of root and shoot components reinforces the importance of root–shoot communication in plant–microbe interactions, as shown previously, such as for camalexin and coumarins (Koprivova et al. 2023; Stassen et al. 2021). The largest cluster with components induced by both BG and CH267 seems to represent the core response, as it links defense-related metabolites with peroxidase proteins and genes involved in plant–microbe interactions. For example, *CAFFEOYL-COA O-METHYLTRANSFERASE* (*CCOAMT*), induced by both strains in our analysis, has been induced by another PGP strain, *Bacillus cereus* D1 (Tsai et al. 2023). WRKY54 is an activator of cell death in immunity and is targeted by various bacterial effectors to suppress its function (Kim et al. 2024). The features identified through the multilevel analysis thus represent promising candidates for further functional studies to better understand the complex responses of plants to microbes.

Conclusions

Our multilevel analysis revealed that the pathogen BG triggered stronger transcriptional reprogramming and proteomic changes in roots than the PGP strain CH267. This supports the idea that plants can distinguish between commensal and pathogenic strains, not at the recognition step alone but through the intensity and extent of downstream responses. We showed that even though only the roots were inoculated, many proteins in the leaves were affected, highlighting root–shoot communication as a central element of the plant–microbe response. Our results reinforce the central role of sulfur metabolism in defense, as both strains induced sulfur-containing metabolites, but the pathogen did so more strongly. In addition, the alterations of metabolites, transcripts, and proteins for sulfur metabolism were accompanied by elevated total sulfur in leaves. We identified a root–exudate rebalancing of metabolites, particularly amino acids and TCA intermediates, indicating that the plants may keep their resources in roots under microbial challenge. Mineral nutrition emerged as an integral part of the immune response and interaction with both PGP and pathogenic strains. Finally, we showed that multilevel integration may reveal hidden regulatory links, such as strong correlations between transcripts, proteins, and metabolites. The integrative analyses with DIABLO uncovered new candidate nodes of regulation and displayed the complexity of the plant response to bacteria on multiple interconnecting layers. These nodes are promising targets for further investigations.

Materials and Methods

Plant material and growth conditions

Arabidopsis thaliana L. accession Col-0 was used for all experiments. The plants were grown in a hydroculture system as described previously (Koprivova et al. 2023). Seeds were surface sterilized with chlorine gas, resuspended in 0.1% agarose, distributed onto square 1- × 1-cm sterile nylon membranes (approximately 30 seeds per sample), and placed in 12-well plates on top of 1 ml of a ½ Murashige Skoog (MS) medium with 0.5% sucrose. The plates were kept for 2 days in 4°C and darkness for stratification and then transferred to 22°C and darkness for a further 3 days to promote etiolation. Afterward, the plates were incubated in a controlled environment under long-day conditions (16 h of light/8 h of dark), 120 μE m^{-2} S^{-1}, and at 22°C for 7 days. The medium was replaced with ½ MS without sucrose, and the plants were incubated for 24 h before inoculation with the bacteria or mock and incubated further under the same conditions for 3 days. The experimental setup is schematically shown in Supplementary Figure S12.

Bacterial strains and cocultivation conditions

For bacterial treatments, CH267 (Haney et al. 2015), obtained from J. R. Dinneny, Stanford University, and BG (Gao et al. 2015), obtained from K.-E. Jäger, Heinrich Heine University Düsseldorf, Germany, were used. The bacteria were kept as glycerol stocks, plated freshly before the experiment on Luria–Bertani plates supplemented with 50 μg/ml ampicillin (CH267) or 25 μg/ml chloramphenicol (BG) and grown at 28 and 30°C, respectively. For inoculation, overnight bacterial cultures were washed two times with sterile 10 mM $MgCl_2$ and diluted to OD_{600} = 0.0001 (CH267) to or OD_{600} = 0.0005 (BG). Each well of the 12-well plate was inoculated with 8 μl of the bacterial suspension or 10 mM $MgCl_2$ as mock. Samples were harvested after 3 days of inoculation, immediately frozen in liquid nitrogen, and kept at −80°C before analysis.

RNA isolation and RNAseq

For RNAseq, the RNA was isolated with PureLink Plant RNA Reagent (Invitrogen, Thermo Scientific, Waltham, MA, U.S.A.), using the small-scale isolation procedure as described in (Zenzen et al. 2024). The RNA samples were further treated with the TURBO DNA-free Kit (Invitrogen, Thermo Scientific) to eliminate DNA, according to the manufacturer's protocol. Purified RNA was sequenced by Novogene (Novogene Co., Cambridge, U.K.) using a non-strand-specific RNA library construction by poly-T mRNA enrichment, random fragmentation, and cDNA synthesis via random hexamer priming. The RNA was sequenced using the Illumina NovaSeq 6000 Sequencing System (Illumina, San Diego, CA, U.S.A.) to produce paired-end 150-bp reads and coverage of 30 to 40 Mio reads per sample in three biological replicates. The adapters from the raw reads were removed by processing with Trimmomatic (Bolger et al. 2014), and the reads were then mapped to the *A. thaliana* reference genome (TAIR10) using HiSAT2 with default parameters (Kim et al. 2019). The resulting reads were then counted with HTseq (Anders et al. 2015) with default parameters and normalized to TPM values. The differential expression analysis was performed with DESeq2 (Love et al. 2014), using $\log_2$ fold change > 1 or $\log_2$ fold change < -1 and an adjusted $P < 0.01$ cut-off to obtain DEGs for further analyses. The Venny platform (https://bioinfogp.cnb.csic.es/tools/venny/index.html) was used to construct the Venn diagrams. GO and KEGG pathway enrichment analyses were performed in the Biomaps app in VirtualPlant (Katari et al. 2010). The graphs were constructed using the SRplot platform (Tang et al. 2023). For mapping the DEGs on metabolic pathways, we used either MapMan 3.6 (Thimm et al. 2004) or ShinyGO 0.82 (Ge et al. 2020) using the Pathview visualization (Luo and Brouwer 2013). The regulation of 25 randomly selected genes was confirmed by comparison of the fold change obtained by RNAseq with the results of qRT-PCR analyses (Supplementary Fig. S13) using the primers described in Supplementary Table S11.

Proteomics

The proteomics analysis was performed exactly as in Berková et al. (2024). Briefly, approximately 10 mg of homogenized freeze-dried plant material was extracted with a methyl tert-butyl ether/methanol/water mixture. Proteomics samples corresponding to 5 µg of proteins were analyzed by nanoflow reverse-phase liquid chromatography-mass spectrometry on a 15-cm C18 Zorbax column (Agilent Technologies, Santa Clara, CA, U.S.A.), a Dionex Ultimate 3000 RSLC nano-UPLC system, and the Orbitrap Fusion Lumos Tribrid Mass Spectrometer (Thermo Fisher Scientific). The measured spectra were recalibrated and searched against the *A. thaliana* ARAPORT 11 database and common contaminants databases using Proteome Discoverer 2.5 (Thermo Fisher Scientific) with algorithms SEQUEST and MS Amanda (Dorfer et al. 2014). The quantitative differences were determined by Minora, employing precursor ion quantification followed by normalization (total area) and calculation of relative peptide/protein abundances. Only proteins with at least two unique peptides were considered. Protein function was predicted by searching sequences against the *A. thaliana* proteome in STRING 11.0 and UniProt (https://www.uniprot.org/). The analysis was done in at least four biological replicates. The mass spectrometry proteomics data were deposited at the ProteomeXchange Consortium via the PRIDE partner repository (Perez-Riverol et al. 2022) with the dataset identifier PXD058537. Statistical evaluation was performed as described for the RNAseq dataset, using an absolute $\log_2$ fold change > 1 and an adjusted $P < 0.01$ as cut-offs to identify the most relevant DAPs for further analyses. Only proteins with more than four values out of the five replicates in at least one condition were considered for the analysis.

Metabolite analysis

Thiols and glucosinolates were determined by standard high-performance liquid chromatography procedures as described in Dietzen et al. (2020). Camalexin was extracted from approximately 10 to 20 mg of plant roots or shoots and determined by high-performance liquid chromatography as described in Koprivova et al. (2019). The untargeted analysis of root metabolites was performed as described in Zenzen et al. (2024) from approximately 30 mg of frozen plant material. The metabolites were derivatized using methoxyamine hydrochloride and N-methyl-N-(trimethylsilyl)trifluoroacetamide and analyzed by gas chromatography coupled with mass spectrometry as previously described (Shim et al. 2020). The identification was performed using the MassHunter Workstation Qualitative Analysis Software (version B.06.00; Agilent Technologies) by comparing the spectra with the NIST14 Mass Spectral Library (https://www.nist.gov/srd/nist-standard-reference-database-1a-v14). Quantitative measurement was achieved by peak integration with MassHunter Workstation Quantitative Analysis Software (version B.08.00), using the internal standard ribitol.

The exudates were freeze-dried in a SpeedVac. The exudates samples were subsequently derivatized as described in Berková et al. (2024) and analyzed using a Q Exactive GC Orbitrap GC-MS/MS mass spectrometer (Thermo Fisher Scientific) coupled to a Trace 1300 Gas Chromatograph (Thermo Fisher Scientific) using a TG-5SILMS column (30 m; 0.25 mm; 0.25 µm; Thermo Fisher Scientific) with a temperature gradient (5 min at 70°C followed by a 9°C gradient in 1 min to 320°C and final incubation for 5 min at 320°C). Data were analyzed by Compound Discoverer 3.3 (Thermo Fisher Scientific) and searched against NIST2014, the GC-Orbitrap Metabolomics library, and an in-house library. Only metabolites that fulfilled identification criteria (score ≥ 85 and $\Delta RI < 1\%$) were included in the final list of identified compounds. The quantitative differences were validated by manual peak assignment in Skyline 19.1 (Pino et al. 2020), using the extracted ion chromatogram (2 ppm tolerance). The analysis was done in four biological replicates.

Elemental analysis

The mineral composition of leaf tissue was determined by inductively coupled plasma mass spectrometry (ICP-MS) from 15 to 20 mg of lyophilized shoot tissue by the CEPLAS Plant Metabolism and Metabolomics Laboratory, University of Cologne, using an Agilent 7700 ICP-MS (Agilent Technologies) (Almario et al. 2017).

Integrative data analysis

The data integration was performed with the shiny application Holomics (Munk et al. 2024) to conduct the DIABLO analysis (Singh et al. 2019). DIABLO uses PLS analysis and generalized canonical correlation analysis to maximize the correlations between multiple omics datasets by selecting a subset of molecular features and discriminating between multiple phenotypic groups. The PLS-DA analyses for each dataset and their correlations was performed using the 'plotDiablo' function. The 'cimDiablo' function was employed to visualize the correlation between components from the different datasets. The hierarchical clustering of the correlation matrix was performed with ClusVis (Metsalu and Vilo 2015).

Data availability

The RNAseq data are available through the NCBI SRA repository under accession number PRJNA1196130. The mass

spectrometry proteomics data were deposited at the ProteomeXchange Consortium with the dataset identifier PXD058537. Other data are included in supplementary tables and/or available from the corresponding author on request.

Acknowledgments

We thank J. R. Dinneny, Stanford University, and K.-E. Jäger, Heinrich Heine Universität Düsseldorf, Germany, for the *Pseudomonas* CH267 and *Burkholderia glumae* PG1 strains; Elisabeth Klemp, Irene Klinkhammer, and Sabine Ambrosius for technical support; and the CEPLAS Metabolism and Metabolomics Laboratory for the analysis of primary metabolites (at Heinrich Heine Universität Düsseldorf) and ionome by ICP-MS (at University of Cologne). The corresponding author acknowledges the use of ChatGPT (OpenAI, San Francisco, CA, U.S.A.) to improve the clarity and readability of the manuscript text. All scientific content, analyses, and interpretations were performed and verified by the authors.

Literature Cited

Almario, J., Jeena, G., Wunder, J., Langen, G., Zuccaro, A., Coupland, G., and Bucher, M. 2017. Root-associated fungal microbiota of nonmycorrhizal *Arabis alpina* and its contribution to plant phosphorus nutrition. Proc. Natl. Acad. Sci. U.S.A. 114:E9403-E9412.

Anders, S., Pyl, P. T., and Huber, W. 2015. HTSeq—A Python framework to work with high-throughput sequencing data. Bioinformatics 31: 166-169.

Aslam, S. N., Newman, M.-A., Erbs, G., Morrissey, K. L., Chinchilla, D., Boller, T., Jensen, T. T., De Castro, C., Ierano, T., Molinaro, A., Jackson, R. W., Knight, M. R., and Cooper, R. M. 2008. Bacterial polysaccharides suppress induced innate immunity by calcium chelation. Curr. Biol. 18:1078-1083.

Bancel, E., Bonnot, T., Davanture, M., Alvarez, D., Zivy, M., Martre, P., Déjean, S., and Ravel, C. 2019. Proteomic data integration highlights central actors involved in einkorn (*Triticum monococcum* ssp. *monococcum*) grain filling in relation to grain storage protein composition. Front. Plant Sci. 10:832.

Berková, V., Berka, M., Štěpánková, L., Kováč, J., Auer, S., Menšíková, S., Ďurkovič, J., Kopřiva, S., Ludwig-Müller, J., Brzobohatý, B., and Černý, M. 2024. The fungus *Acremonium alternatum* enhances salt stress tolerance by regulating host redox homeostasis and phytohormone signaling. Physiol. Plant. 176:e14328.

Bolger, A. M., Lohse, M., and Usadel, B. 2014. Trimmomatic: A flexible trimmer for Illumina sequence data. Bioinformatics 30:2114-2120.

Browne, L. M., Conn, K. L., Ayert, W. A., and Tewari, J. P. 1991. The camalexins: New phytoalexins produced in the leaves of *Camelina sativa* (cruciferae). Tetrahedron 47:3909-3914.

Burton-Pimentel, K. J., Pimentel, G., Hughes, M., Michielsen, C. C. J. R., Fatima, A., Vionnet, N., Afman, L. A., Roche, H. M., Brennan, L., Ibberson, M., and Vergères, G. 2021. Discriminating dietary responses by combining transcriptomics and metabolomics data in nutrition intervention studies. Mol. Nutr. Food Res. 65:2000647.

Campos-Soriano, L., García-Martínez, J., and San Segundo, B. 2012. The arbuscular mycorrhizal symbiosis promotes the systemic induction of regulatory defence-related genes in rice leaves and confers resistance to pathogen infection. Mol. Plant Pathol. 13:579-592.

Castellanos, L., Naranjo-Gaybor, S. J., Forero, A. M., Morales, G., Wilson, E. G., Ramos, F. A., and Choi, Y. H. 2020. Metabolic fingerprinting of banana passion fruits and its correlation with quorum quenching activity. Phytochemistry 172:112272.

de Jonge, R., van Esse, H. P., Kombrink, A., Shinya, T., Desaki, Y., Bours, R., van der Krol, S., Shibuya, N., Joosten, M. H. A. J., and Thomma, B. P. H. J. 2010. Conserved fungal LysM effector Ecp6 prevents chitin-triggered immunity in plants. Science 329:953-955.

Devos, S., Laukens, K., Deckers, P., Van Der Straeten, D., Beeckman, T., Inzé, D., Van Onckelen, H., Witters, E., and Prinsen, E. 2006. A hormone and proteome approach to picturing the initial metabolic events during *Plasmodiophora brassicae* infection on *Arabidopsis*. Mol. Plant-Microbe Interact. 19:1431-1443.

de Zélicourt, A., Synek, L., Saad, M. M., Alzubaidy, H., Jalal, R., Xie, Y., Andrés-Barrao, C., Rolli, E., Guerard, F., Mariappan, K. G., Daur, I., Colcombet, J., Benhamed, M., Depaepe, T., Van Der Straeten, D., and Hirt, H. 2018. Ethylene induced plant stress tolerance by *Enterobacter* sp. SA187 is mediated by 2-keto-4-methylthiobutyric acid production. PLoS Genet. 14:e1007273.

Dietzen, C., Koprivova, A., Whitcomb, S. J., Langen, G., Jobe, T. O., Hoefgen, R., and Kopriva, S. 2020. The transcription factor EIL1 participates in the regulation of sulfur-deficiency response. Plant Physiol. 184:2120-2136.

Dorfer, V., Pichler, P., Stranzl, T., Stadlmann, J., Taus, T., Winkler, S., and Mechtler, K. 2014. MS Amanda, a universal identification algorithm optimized for high accuracy tandem mass spectra. J. Proteome Res. 13:3679-3684.

Esparza-Reynoso, S., Ayala-Rodríguez, J. Á., and López-Bucio, J. 2024. *Pseudomonas putida* configures *Arabidopsis* root architecture through modulating the sensing systems for phosphate and iron acquisition. Plant Sci. 342:112028.

Fan, J., Crooks, C., Creissen, G., Hill, L., Fairhurst, S., Doerner, P., and Lamb, C. 2011. *Pseudomonas sax* genes overcome aliphatic isothiocyanate-mediated non-host resistance in *Arabidopsis*. Science 331:1185-1188.

Gao, R., Krysciak, D., Petersen, K., Utpatel, C., Knapp, A., Schmeisser, C., Daniel, R., Voget, S., Jaeger, K.-E., and Streit, W. R. 2015. Genome-wide RNA sequencing analysis of quorum sensing-controlled regulons in the plant-associated *Burkholderia glumae* PG1 strain. Appl. Environ. Microbiol. 81:7993-8007.

Ge, S. X., Jung, D., and Yao, R. 2020. ShinyGO: A graphical gene-set enrichment tool for animals and plants. Bioinformatics 36:2628-2629.

Ghitti, E., Rolli, E., Crotti, E., and Borin, S. 2022. Flavonoids are intra- and inter-kingdom modulator signals. Microorganisms 10:2479.

Glawischnig, E. 2007. Camalexin. Phytochemistry 68:401-406.

Ham, J. H., Melanson, R. A., and Rush, M. C. 2011. *Burkholderia glumae*: Next major pathogen of rice? Mol. Plant Pathol. 12:329-339.

Haney, C. H., Samuel, B. S., Bush, J., and Ausubel, F. M. 2015. Associations with rhizosphere bacteria can confer an adaptive advantage to plants. Nat. Plants 1:15051.

Haney, C. H., Wiesmann, C. L., Shapiro, L. R., Melnyk, R. A., O'Sullivan, L. R., Khorasani, S., Xiao, L., Han, J., Bush, J., Carrillo, J., Pierce, N. E., and Ausubel, F. M. 2018. Rhizosphere-associated *Pseudomonas* induce systemic resistance to herbivores at the cost of susceptibility to bacterial pathogens. Mol. Ecol. 27:1833-1847.

Harbort, C. J., Hashimoto, M., Inoue, H., Niu, Y., Guan, R., Rombolà, A. D., Kopriva, S., Voges, M. J. E. E. E., Sattely, E. S., Garrido-Oter, R., and Schulze-Lefert, P. 2020. Root-secreted coumarins and the microbiota interact to improve iron nutrition in *Arabidopsis*. Cell Host Microbe 28:825-837.

Herlihy, J. H., Long, T. A., and McDowell, J. M. 2020. Iron homeostasis and plant immune responses: Recent insights and translational implications. J. Biol. Chem. 295:13444-13457.

Huang, A. C., Jiang, T., Liu, Y.-X., Bai, Y.-C., Reed, J., Qu, B., Goossens, A., Nützmann, H.-W., Bai, Y., and Osbourn, A. 2019. A specialized metabolic network selectively modulates *Arabidopsis* root microbiota. Science 364:eaau6389.

Hucklenbroich, J., Gigolashvili, T., Koprivova, A., Spohr, P., Chegini, M. N., Klau, G. W., Kopriva, S., and Nakano, R. T. 2021. Rhizobiales commensal bacteria promote *Arabidopsis thaliana* root growth via host sulfated peptide pathway. bioRxiv 444716.

Jacoby, R. P., Koprivova, A., and Kopriva, S. 2021. Pinpointing secondary metabolites that shape the composition and function of the plant microbiome. J. Exp. Bot. 72:57-69.

Jain, A., Sarsaiya, S., Singh, R., Gong, Q., Wu, Q., and Shi, J. 2024. Omics approaches in understanding the benefits of plant-microbe interactions. Front. Microbiol. 15:1391059.

Ji, L., Yang, X., and Qi, F. 2022. Distinct responses to pathogenic and symbionic microorganisms: The role of plant immunity. Int. J. Mol. Sci. 23:10427.

Katari, M. S., Nowicki, S. D., Aceituno, F. F., Nero, D., Kelfer, J., Thompson, L. P., Cabello, J. M., Davidson, R. S., Goldberg, A. P., Shasha, D. E., Coruzzi, G. M., and Gutiérrez, R. A. 2010. VirtualPlant: A software platform to support systems biology research. Plant Physiol. 152: 500-515.

Kertesz, M. A., and Mirleau, P. 2004. The role of soil microbes in plant sulphur nutrition. J. Exp. Bot. 55:1939-1945.

Kim, D., Paggi, J. M., Park, C., Bennett, C., and Salzberg, S. L. 2019. Graph-based genome alignment and genotyping with HISAT2 and HISAT-genotype. Nat. Biotechnol. 37:907-915.

Kim, H., Kim, J., Choi, D. S., Kim, M.-S., Deslandes, L., Jayaraman, J., and Sohn, K. H. 2024. Molecular basis for the interference of the Arabidopsis WRKY54-mediated immune response by two sequence-unrelated bacterial effectors. Plant J. 118:839-855.

Kliebenstein, D. J., Rowe, H. C., and Denby, K. J. 2005. Secondary metabolites influence Arabidopsis/*Botrytis* interactions: Variation in host production and pathogen sensitivity. Plant J. 44:25-36.

Koprivova, A., and Kopriva, S. 2022. Plant secondary metabolites altering root microbiome composition and function. Curr. Opin. Plant Biol. 67:102227.

Koprivova, A., Schuck, S., Jacoby, R. P., Klinkhammer, I., Welter, B., Leson, L., Martyn, A., Nauen, J., Grabenhorst, N., Mandelkow, J. F., Zuccaro, A., Zeier, J., and Kopriva, S. 2019. Root-specific camalexin biosynthesis controls the plant growth-promoting effects of multiple bacterial strains. Proc. Natl. Acad. Sci. U.S.A. 116:15735-15744.

Koprivova, A., Schwier, M., Volz, V., and Kopriva, S. 2023. Shoot-root interaction in control of camalexin exudation in Arabidopsis. J. Exp. Bot. 74:2667-2679.

Kwon, Y. S., Lee, D. Y., Rakwal, R., Baek, S.-B., Lee, J. H., Kwak, Y.-S., Seo, J.-S., Chung, W. S., Bae, D.-W., and Kim, S. G. 2016. Proteomic analyses of the interaction between the plant-growth promoting rhizobacterium *Paenibacillus polymyxa* E681 and *Arabidopsis thaliana*. Proteomics 16:122-135.

Lahrmann, U., Strehmel, N., Langen, G., Frerigmann, H., Leson, L., Ding, Y., Scheel, D., Herklotz, S., Hilbert, M., and Zuccaro, A. 2015. Mutualistic root endophytism is not associated with the reduction of saprotrophic traits and requires a noncompromised plant innate immunity. New Phytol. 207:841-857.

Love, M. I., Huber, W., and Anders, S. 2014. Moderated estimation of fold change and dispersion for RNA-seq data with DESeq2. Genome Biol. 15:550.

Luo, W., and Brouwer, C. 2013. Pathview: An R/Bioconductor package for pathway-based data integration and visualization. Bioinformatics 29:1830-1831.

Magbanua, Z. V., Arick, M., II, Buza, T., Hsu, C.-Y., Showmaker, K. C., Chouvarine, P., Deng, P., Peterson, D. G., and Lu, S. 2014. Transcriptomic dissection of the rice – *Burkholderia glumae* interaction. BMC Genomics 15:755.

Maier, B. A., Kiefer, P., Field, C. M., Hemmerle, L., Bortfeld-Miller, M., Emmenegger, B., Schäfer, M., Pfeilmeier, S., Sunagawa, S., Vogel, C. M., and Vorholt, J. A. 2021. A general non-self response as part of plant immunity. Nat. Plants 7:696-705.

Marzorati, F., Rossi, R., Bernardo, L., Mauri, P., Silvestre, D. D., Lauber, E., Noël, L. D., Murgia, I., and Morandini, P. 2023. *Arabidopsis thaliana* early foliar proteome response to root exposure to the rhizobacterium *Pseudomonas simiae* WCS417. Mol. Plant-Microbe Interact. 36: 737-748.

Metsalu, T., and Vilo, J. 2015. ClustVis: A web tool for visualizing clustering of multivariate data using Principal Component Analysis and heatmap. Nucleic Acids Res. 43:W566-W570.

Moormann, J., Heinemann, B., and Hildebrandt, T. M. 2022. News about amino acid metabolism in plant–microbe interactions. Trends Biochem. Sci. 47:839-850.

Mukherjee, A., Han, L., Mukhopadhyay, S., Kopriva, S., and Swarup, S. 2025. Sulfur traits in the plant microbiome: Implications for sustainable agriculture. Trends Microbiol. 33:635-649.

Munk, K., Ilina, D., Ziemba, L., Brader, G., and Molin, E. M. 2024. Holomics - a user-friendly R shiny application for multi-omics data integration and analysis. BMC Bioinform. 25:93.

Nguyen, N. H., Trotel-Aziz, P., Clément, C., Jeandet, P., Baillieul, F., and Aziz, A. 2022. Camalexin accumulation as a component of plant immunity during interactions with pathogens and beneficial microbes. Planta 255:116.

Nobori, T., Cao, Y., Entila, F., Dahms, E., Tsuda, Y., Garrido-Oter, R., and Tsuda, K. 2022. Dissecting the cotranscriptome landscape of plants and their microbiota. EMBO Rep. 23:e55380.

Pangesti, N., Reichelt, M., van de Mortel, J. E., Kapsomenou, E., Gershenzon, J., van Loon, J. J. A., Dicke, M., and Pineda, A. 2016. Jasmonic acid and ethylene signaling pathways regulate glucosinolate levels in plants during rhizobacteria-induced systemic resistance against a leaf-chewing herbivore. J. Chem. Ecol. 42:1212-1225.

Paries, M., and Gutjahr, C. 2023. The good, the bad, and the phosphate: Regulation of beneficial and detrimental plant–microbe interactions by the plant phosphate status. New Phytol. 239:29-46.

Perez-Riverol, Y., Bai, J., Bandla, C., García-Seisdedos, D., Hewapathirana, S., Kamatchinathan, S., Kundu, D. J., Prakash, A., Frericks-Zipper, A., Eisenacher, M., Walzer, M., Wang, S., Brazma, A., and Vizcaino, J. A. 2022. The PRIDE database resources in 2022: A hub for mass spectrometry-based proteomics evidences. Nucleic Acids Res. 50:D543-D552.

Pieterse, C. M. J., van Wees, S. C. M., Hoffland, E., van Pelt, J. A., and van Loon, L. C. 1996. Systemic resistance in Arabidopsis induced by biocontrol bacteria is independent of salicylic acid accumulation and pathogenesis-related gene expression. Plant Cell 8:1225-1237.

Pino, L. K., Searle, B. C., Bollinger, J. G., Nunn, B., MacLean, B., and MacCoss, M. J. 2020. The Skyline ecosystem: Informatics for quantitative mass spectrometry proteomics. Mass Spectrom. Rev. 39: 229-244.

Poupin, M. J., Timmermann, T., Vega, A., Zuñiga, A., and González, B. 2013. Effects of the plant growth-promoting bacterium *Burkholderia phytofirmans* PsJN throughout the life cycle of *Arabidopsis thaliana*. PLoS One 8:e69435.

Rausch, T., and Wachter, A. 2005. Sulfur metabolism: A versatile platform for launching defence operations. Trends Plant Sci. 10:503-509.

Salas-González, I., Reyt, G., Flis, P., Custódio, V., Gopaulchan, D., Bakhoum, N., Dew, T. P., Suresh, K., Franke, R. B., Dangl, J. L., Salt, D. E., and Castrillo, G. 2021. Coordination between microbiota and root endodermis supports plant mineral nutrient homeostasis. Science 371:eabd0695.

Sasse, J., Martinoia, E., and Northen, T. 2018. Feed your friends: Do plant exudates shape the root microbiome? Trends Plant Sci. 23:25-41.

Shim, S.-H., Lee, S.-K., Lee, D.-W., Brilhaus, D., Wu, G., Ko, S., Lee, C.-H., Weber, A. P. M., and Jeon, J.-S. 2020. Loss of function of rice plastidic glycolate/glycerate translocator 1 impairs photorespiration and plant growth. Front. Plant Sci. 10:1726.

Singh, A., Shannon, C. P., Gautier, B., Rohart, F., Vacher, M., Tebbutt, S. J., and Lê Cao, K.-A. 2019. DIABLO: An integrative approach for identifying key molecular drivers from multi-omics assays. Bioinformatics 35:3055-3062.

Song, W.-Y., Choi, K. S., Kim, D. Y., Geisler, M., Park, J., Vincenzetti, V., Schellenberg, M., Kim, S. H., Lim, Y. P., Noh, E. W., Lee, Y., and Martinoia, E. 2010. *Arabidopsis* PCR2 is a zinc exporter involved in both zinc extrusion and long-distance zinc transport. Plant Cell 22:2237-2252.

Stassen, M. J. J., Hsu, S.-H., Pieterse, C. M. J., and Stringlis, I. A. 2021. Coumarin communication along the microbiome-root-shoot axis. Trends Plant Sci. 26:169-183.

Stringlis, I. A., Yu, K., Feussner, K., de Jonge, R., Van Bentum, S., Van Verk, M. C., Berendsen, R. L., Bakker, P. A. H. M., Feussner, I., and Pieterse, C. M. J. 2018. MYB72-dependent coumarin exudation shapes root microbiome assembly to promote plant health. Proc. Natl. Acad. Sci. U.S.A. 115:E5213-E5222.

Tang, D., Chen, M., Huang, X., Zhang, G., Zeng, L., Zhang, G., Wu, S., and Wang, Y. 2023. SRplot: A free online platform for data visualization and graphing. PLoS One 18:e0294236.

Teixeira, P. J. P. L., Colaianni, N. R., Law, T. F., Conway, J. M., Gilbert, S., Li, H., Salas-González, I., Panda, D., Del Risco, N. M., Finkel, O. M., Castrillo, G., Mieczkowski, P., Jones, C. D., and Dangl, J. L. 2021. Specific modulation of the root immune system by a community of commensal bacteria. Proc. Natl. Acad. Sci. U.S.A. 118:e2100678118.

Thimm, O., Bläsing, O., Gibon, Y., Nagel, A., Meyer, S., Krüger, P., Selbig, J., Müller, L. A., Rhee, S. Y., and Stitt, M. 2004. MAPMAN: A user-driven tool to display genomics data sets onto diagrams of metabolic pathways and other biological processes. Plant J. 37:914-939.

Thoms, D., Liang, Y., and Haney, C. H. 2021. Maintaining symbiotic homeostasis: How do plants engage with beneficial microorganisms while at the same time restricting pathogens? Mol. Plant-Microbe Interact. 34:462-469.

Tsai, S.-H., Hsiao, Y.-C., Chang, P. E., Kuo, C.-E., Lai, M.-C., and Chuang, H.-w. 2023. Exploring the biologically active metabolites produced by *Bacillus cereus* for plant growth promotion, heat stress tolerance, and resistance to bacterial soft rot in *Arabidopsis*. Metabolites 13:676.

Vilchez, J. I., Yang, Y., He, D., Zi, H., Peng, L., Lv, S., Kaushal, R., Wang, W., Huang, W., Liu, R., Lang, Z., Miki, D., Tang, K., Paré, P. W., Song, C.-P., Zhu, J.-K., and Zhang, H. 2020. DNA demethylases are required for *myo*-inositol-mediated mutualism between plants and beneficial rhizobacteria. Nat. Plants 6:983-995.

Wang, W., Liu, J., Mishra, B., Mukhtar, M. S., and McDowell, J. M. 2022. Sparking a sulfur war between plants and pathogens. Trends Plant Sci. 27:1253-1265.

Witzel, K., Üstün, S., Schreiner, M., Grosch, R., Börnke, F., and Ruppel, S. 2017. A proteomic approach suggests unbalanced proteasome functioning induced by the growth-promoting bacterium *Kosakonia radicincitans* in Arabidopsis. Front. Plant Sci. 8:661.

Yang, Q., Li, Z., Guan, K., Wang, Z., Tang, X., Hong, Y., Liu, Z., Zhai, J., Huang, A., Long, Y., and Song, Y. 2025. Comparative single-nucleus RNA-seq analysis revealed localized and cell type-specific pathways governing root-microbiome interactions. Nat. Commun. 16:3169.

Zenzen, I., Cassol, D., Westhoff, P., Kopriva, S., and Ristova, D. 2024. Transcriptional and metabolic profiling of sulfur starvation response in two monocots. BMC Plant Biol. 24:257.

Zhao, C., Wang, H., Lu, Y., Hu, J., Qu, L., Li, Z., Wang, D., He, Y., Valls, M., Coll, N. S., Chen, Q., and Lu, H. 2019. Deep sequencing reveals early reprogramming of *Arabidopsis* root transcriptomes upon *Ralstonia solanacearum* infection. Mol. Plant-Microbe Interact. 32:813-827.

Zipfel, C., and Oldroyd, G. E. D. 2017. Plant signalling in symbiosis and immunity. Nature 543:328-336.